

Improvement of the Cluster-Level Spatial Consistency of Channel Simulator with Reference Points Transition Method

Chi Wu, Yiming Zhu, Wenjin Wang, *Member, IEEE*, Cheng-Xiang Wang, *Fellow, IEEE*, and Xiqi Gao, *Fellow, IEEE*

Abstract—Spatial consistency is a basic physical characteristic of the wireless channel because the neighboring spatial positions share similar clusters, resulting in the spatial correlations of both large-scale parameters (LSPs) and small-scale parameters (SSPs). Although the existing geometry-based stochastic channel model (GSCM)-based channel simulator try to realize the spatial consistency of the channel parameters by the correlated map method or the sum-of-sinusoids (SOS) method, such a stochastic approach also results in that the change of cluster positions calculated by the SSPs appears considerable even in closely neighboring spatial positions, which violates the wide-sense stationary (WSS) conditions over a short distance. To further improve the cluster-level spatial consistency, we investigate the pattern of change of the root mean square (RMS)-delay spread (DS) and derive the continuity of RMS-DS in the entire space. Taking the continuity of RMS-DS as the optimization goal, we determine the change of clusters of the channel, i.e., cluster appearance and disappearance, when the spatial position of mobile terminal (MT) changes and propose the reference points (RPs) transition method. Specifically, we firstly choose the RPs in the target area according to the correlation distance, then generate the channels of RPs by the SOS method stochastically, and finally obtain the channel of MT through the transitions between the RPs deterministically. Simulation results demonstrate that the channel simulator with the proposed RPs transition method can achieve the spatial consistency of LSPs, SSPs, and clusters in the entire 2D or 3D space.

Index Terms—Channel model, spatial consistency, wireless channel simulator, cluster appearance and disappearance

I. INTRODUCTION

A proper channel model is significant for simulating the new concepts in wireless communication networks, especially in

Manuscript received June 17, 2021; revised November 8, 2021 and February 18, 2022; accepted March 15, 2022. Date of publication xx, xxxx; date of current version March 20, 2022. This work was supported in part by the National Key R&D Program of China under Grant 2019YFB1803102, and in part by the Jiangsu Province Basic Research Project under Grant BK20192002, the National Natural Science Foundation of China (NSFC) under Grant 61960206006, the Frontiers Science Center for Mobile Information Communication and Security, the High Level Innovation and Entrepreneurial Research Team Program in Jiangsu, the High Level Innovation and Entrepreneurial Talent Introduction Program in Jiangsu, and the EU H2020 RISE TESTBED2 project under Grant 872172. The associate editor coordinating the review of this article and approving it for publication was Yiqing Zhou. (*Chi Wu and Yiming Zhu contributed equally to this work.*) (Corresponding author: Wenjin Wang.)

Copyright (c) 2015 IEEE. Personal use of this material is permitted. However, permission to use this material for any other purposes must be obtained from the IEEE by sending a request to pubs-permissions@ieee.org.

C. Wu, Y. Zhu, W. Wang, C.-X. Wang, and X. Q. Gao are with the National Mobile Communications Research Laboratory, Southeast University, Nanjing 210096, China, and also with the Purple Mountain Laboratories, Nanjing 211111, China (e-mail: chiwu@seu.edu.cn; zhuym@seu.edu.cn; wangwj@seu.edu.cn; chxwang@seu.edu.cn; xqgao@seu.edu.cn).

the most advanced fifth generation (5G) communication. From the perspective of the modeling approach, channel models can be classified into deterministic classes and stochastic classes [1], [2]. Relying on the precise information of site-specific virtual propagation environments, deterministic channel models such as the ray tracer [3] predict the channels accurately by solving the Maxwell equations or the approximate ones at the expense of massive site-specific channel measurements and high computational complexity. In contrast, stochastic channel models utilize certain probability distributions determined by the channel measurements to describe channel parameters so that they can be applied to various scenarios and are mathematically tractable with relatively low accuracy. Considering the complexity and applicability, we focus our attention on the stochastic channel models.

There are already many reliable geometry-based stochastic channel models (GSCMs) for mobile wireless communication systems, e.g., the Third Generation Partnership Project (3GPP) channel models [4]–[6], the Wireless World Initiative for New Radio (WINNER) channel model [7], the Mobile and Wireless Communications Enablers for the Twenty-twenty Information Society (METIS) channel model [8], the MillimeterWave Based Mobile Radio Access Network for Fifth Generation Integrated Communications (mmMAGIC) channel model [9], the Quasi Deterministic Radio Channel Generator (QuaDRiGa) [10], and the European Cooperation in Science and Technology (COST) 2100 channel model [11], [12]. Spatial consistency is an inherent physical characteristic of the wireless channel, which is caused by the similar scattering environment around the neighboring spatial positions. It leads to spatial correlations of small-scale parameters (SSPs), large-scale parameters (LSPs), and clusters between channels in neighboring spatial positions [13]–[16].¹ Therefore, the extension of spatial consistency in the channel simulator is important for the evaluation of space-related concepts.

The existing channel models have already made their effort to model spatial consistency. The 3GPP spatial channel model (SCM) proposes a two-dimensional (2D) spatial channel model for system-level simulations which implements intra-site correlations between different LSPs, e.g., delay spread (DS), angle spread (AS), and shadow fading (SF) [4]. In the WINNER model [7], the LSPs at different positions are further

¹In GSCMs, SSPs refer to the low-level channel parameters, such as the number of clusters, cluster power, cluster angles, cluster delays, and so on. LSPs represent the high-level parameters generally characterized by the second moments of SSPs.

correlated according to the distance between the positions of mobile terminals (MTs). The correlations of LSPs are modeled using the measured data from the known positions and usually have exponential decay over distance. Then channel parameters are generated randomly and independently from measured distribution functions for different MTs based on a 2D modeling approach. The 3GPP three-dimensional (3D) SCM [5] and the 3GPP new radio (NR) channel model [6] provide additional flexibility for the elevation dimension, thereby allowing a 3D modeling approach. Similar to the WINNER model, the 3GPP 3D SCM and the 3GPP NR channel model implement the correlated LSPs using the distance-based correlations. In addition, the 3GPP NR channel model introduces a spatial consistency procedure to generate cluster-specific and ray-specific random variables for drop-based simulations. To support the spatially correlated LSPs in the device-to-device (D2D) scenarios, the METIS channel model proposes the sum-of-sinusoids (SOS) method [17], [18] with low time and space complexity [8]. The mmMAGIC channel model utilizes the extended Saleh-Valenzuela (SV) model [19] to characterize the clusters and rays in both spatial and temporal domains. Besides, the numbers and arrival rates of clusters and rays are modeled as random variables and Poisson processes, respectively [9]. The QuaDRiGa adopts the SOS spatial consistency model in which channel parameters as spatially correlated stochastic processes are approximated as the SOS functions of 3D coordinates [20], [21].² Specifically, the initial LSPs and SSPs are firstly calculated by the SOS method. Then, the scaling operations are implemented to generate the actual SSPs which fulfill the requirements of LSPs. Finally, the cluster positions are calculated by using the actual SSPs. The COST 2100 channel model interpolates spatial consistency in a different way: it first generates the propagation environment with fixed cluster locations, then the channel is determined by the clusters which can be “seen” by the MT [11]. Thus the closely located MTs can share a similar environment in the COST 2100 channel model.

The spatial consistency of the channel over a local space is an essential prerequisite for validations of space-related concepts, e.g., the positioning technology [22]–[25] and the beam tracking technology [13]. On the one hand, spatial consistency requires that any two channels at geographically neighboring locations are correlated. On the other hand, spatial consistency requires that the LSPs, SSPs, and clusters of the channel and geographic location are in one-to-one correspondence because of the unique surrounding environment. The above two requirements of spatial consistency have been realized in the COST 2100 channel model. However, as a cluster-level channel model, the COST 2100 channel model still lacks some important parameter information to parameterize the channel in many scenarios. On the contrary, the existing GSCM-based channel simulators such as the QuaDRiGa are system-level and can simulate enormous scenarios benefiting from sufficient

²In the SOS method, since the neighboring spatial positions share similar clusters, both LSPs and SSPs as stochastic processes should vary in a continuous and realistic manner as a function of spatial positions. In other words, all parameters that determine the propagation environment are derived from spatially correlated stochastic processes.

measurements. Although such a stochastic approach tries to realize the continuous changes of channel parameters over space by the correlated map method or the SOS method, it ignores the spatial consistency of clusters. The cluster positions calculated by the SSPs appear considerably different even over a short distance between two MTs. Sometimes, the distance between the cluster positions of two neighboring MTs exceeds that between two MTs by several orders of magnitude, violating the wide-sense stationary (WSS) conditions, i.e., the cluster positions are approximately the same for closely neighboring spatial positions [21]. Hence, the existing GSCM-based channel simulators still lack spatial consistency at the cluster level.

In this paper, we propose a reference points (RPs) transition method to realize the spatial consistency of the channel simulator at the LSP, SSP, and cluster level over the entire space. We first investigate two characteristics of spatial consistency: 1) The correlation distance [7], [13] is introduced as the spacing between the RPs so that the channels of RPs are mutually independent. At the cluster level, when the MT’s position changes from one RP to another RP, the clusters “seen” by the MT evolve gradually from the clusters of the old RP to those of the new one. 2) According to the circular scattering model proposed in [26], [27], the change of the root mean square (RMS)-DS over the space is derived to be continuous and smooth, and the RPs transition can be implemented to realize cluster appearance and disappearance based on this. Combining these two characteristics, we propose the RPs transition method to improve the cluster-level spatial consistency. Specifically, the RPs are firstly evenly selected in the target area according to the correlation distance. Then a stochastic part generates LSPs and SSPs for these RPs, of which the 2D or 3D positions of the surrounding clusters are calculated and stored. Next, transitions between the RPs are implemented to determine the clusters and the cluster powers for the MT. Finally, the cluster delays and angles are updated based on the geographical calculation to obtain the spatial evolutions of LSPs and SSPs. To summarize, our contributions are as follows:

- 1) Starting from the widely used circular scattering model, we derive that the RMS-DS varies continuously and smoothly over the target area when the number of subpaths is quite large. It inspires us that the RMS-DS variation curve over the space is still around an ideal continuous curve with finite subpaths.
- 2) From two perspectives: the evolution of the RMS-DS and the evolution of the clusters, we propose the RPs transition method to realize the spatial consistency of LSPs, SSPs, and clusters in the entire 2D or 3D space.

The rest of the paper is organized as follows: In Section II, we investigate the characteristics of the channel spatial consistency. Section III describes the realization of spatial consistency. Section IV then uses simulation to validate the performance of the channel simulator with RPs transition method. In Section V, we summarize the paper.

TABLE I: The Range of Correlation Distances and Number of Subpaths in Different Scenarios [6]

Scenario	Range of correlation distance	Number of subpaths
UMi LOS	7 ~ 15 m	221
UMi NLOS	9 ~ 13 m	380
UMa LOS	12 ~ 30 m	221
UMa NLOS	40 ~ 50 m	400

II. CHARACTERISTICS OF SPATIAL CONSISTENCY

The concept of correlation distance has been introduced to describe the correlations of LSPs over the distance in previous literature [7], [13]. An intuitive explanation is that the surrounding clusters are almost completely different when the distance between two MTs is larger than the largest correlation distance. Hence, it is reasonable to confine the investigation of the spatial consistency within the correlation distance. To characterize the transition of the channel, i.e., cluster appearance and disappearance, over the space, we then investigate the changing pattern of RMS-DS with the MT's motion.

A. Correlation Distance

Due to the consistency of the scattering environment, the LSPs of the two channels at adjacent positions are correlated, and these correlations will gradually decrease when the distance between them increases. Then the correlation distance of the LSP is introduced: when the distance of two spatial positions is larger than the correlation distance, the corresponding LSPs of the two channels are statistically independent of each other. At the cluster level, the clusters "seen" by two MTs are completely different when the distance between two MTs is larger than the correlation distance. For channel generation, the WINNER channel model introduces the channel segment as a period of quasi-stationarity in which the LSPs do not change considerably [7]. The Quadriga follows the concept of the channel segment and sets the length of channel segment as the average correlation distance of each LSP. As such, the channels at the beginning and the end of the channel segment are generated independently. The correlation distances are different for different scenarios. The range of correlation distances in several scenarios referring to the 3GPP NR document [6] is listed in Table I.

B. Continuity of RMS-DS

As the root of the second central moment of the normalized power delay profile (PDP), RMS-DS is an important LSP used to measure the multipath richness of a communication channel related to the number of clusters, cluster delays, and cluster powers [28]. To investigate the pattern of RMS-DS change over space, we first look into a widely used spatial channel scattering model. In fixed wireless communication context, the base station (BS) is usually elevated at a very high altitude and seldom obstructed. Thus the multipath components are mainly determined by scatterers surrounding the MT. The circular scattering model assumes that the scatterers are uniformly and

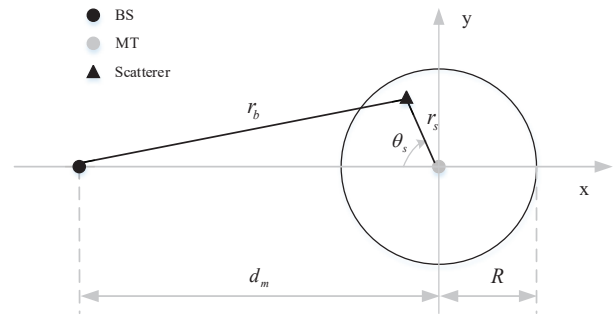


Fig. 1: Circular scattering model with radius R .

independently distributed within a circle around the MT, and only a single scatterer is considered for each non-line of sight (NLOS) path [26], [27], as shown in Fig. 1. Starting from the circular scattering model, we present the changing pattern of RMS-DS over space as in Theorem 1.

Theorem 1: When the number of subpaths is quite large, the RMS-DS varies continuously over the target space. Denote the RMS-DS of the m th MT at the position \mathbf{a}_m as $D(\mathbf{a}_m)$. Suppose \mathbf{a}_0 is an arbitrary position in the space, then the limit of $D(\mathbf{a}_m)$ exists and equals to $D(\mathbf{a}_0)$ when $\mathbf{a}_m \rightarrow \mathbf{a}_0$, given as

$$\lim_{\mathbf{a}_m \rightarrow \mathbf{a}_0} D(\mathbf{a}_m) = D(\mathbf{a}_0). \quad (1)$$

Proof: See appendix A. \square

Remark 1: Theorem 1 demonstrates the continuity of RMS-DS over the space under the assumption that the number of subpaths is quite large. It inspires us that when the number of subpaths is finite, the RMS-DS variation curve is still around an ideal continuous curve. The number of subpaths in different 3GPP scenarios [6] are listed in Table I.

Remark 2: Through carefully setting the RP spacing, the RMS-DS variation curve between two adjacent RPs can be approximated as a continuous straight line. The detailed setting of RPs is described in Section III-A.

III. REALIZATION OF SPATIAL CONSISTENCY

Since the existing channel simulators are system-level and can simulate enormous scenarios benefiting from sufficient measurements, we further realize the spatial consistency at the cluster level besides the LSP and SSP levels over the entire space based on the QuaDRiGa. Fig. 2 shows the overall structure of the channel simulator with the proposed RPs transition method, where the gray blocks represent our modifications to realize spatial consistency. The fixation of

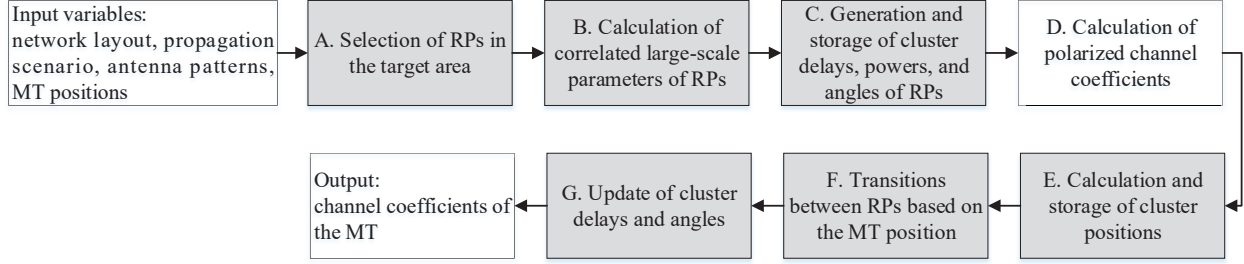


Fig. 2: Steps of the generation of channel coefficients

the scattering environment is incorporated in steps A, B, C, and E. The spatial transition is incorporated in steps F and G.

We implement the spatial consistency from two perspectives: the evolution of the RMS-DS and the evolution of the clusters. The RMS-DS is a significant LSP used to measure the multipath richness of wireless channel. Assume the current position of the m th MT is \mathbf{a}_m , the movement of the MT is represented by a vector $\Delta\mathbf{a}_m$. At the next position $\mathbf{a}_m + \Delta\mathbf{a}_m$, the RMS-DS is evolved as

$$D(\mathbf{a}_m) \xrightarrow{E} D(\mathbf{a}_m + \Delta\mathbf{a}_m), \quad (2)$$

where the operator \xrightarrow{E} denotes the evolution via space. Another important phenomenon of the wireless channel is the birth and death of cluster [29], [30]. To introduce such a physical phenomenon, we assume each cluster only survives in a small geographical area, a.k.a., survival space. Then we pair the new clusters and the old clusters and assume the paired ones have the same survival space. With the motion of MT, the new clusters gradually ramp up and the old ones gradually ramp down until the new ones completely replace the old ones. Let $\alpha_n(\mathbf{a}_m)$ be the complex channel gain corresponding to the n th paired clusters of the MT at position \mathbf{a}_m . We represent the evolution of the complex channel gain at the next position $\mathbf{a}_m + \Delta\mathbf{a}_m$ as

$$\begin{aligned} \alpha_{\text{old},n}(\mathbf{a}_m) &\xrightarrow{E} \alpha_{\text{old},n}(\mathbf{a}_m + \Delta\mathbf{a}_m), \\ \alpha_{\text{new},n}(\mathbf{a}_m) &\xrightarrow{E} \alpha_{\text{new},n}(\mathbf{a}_m + \Delta\mathbf{a}_m). \end{aligned} \quad (3)$$

To realize the channel evolutions described in (2) and (3), we first choose a series of RPs in the target area, and a stochastic part generates LSPs and SSPs for these RPs. Then transitions among these RPs are implemented, and the cluster powers and phases are calculated to generate the channel of MT. Finally, the cluster delays and angles are updated based on the geographical calculation in the fixed scattering environment.

A. Selection of RPs and Generation of LSPs of RPs

In the proposed RPs transition method, the RPs are evenly selected in the target area. Specifically, the positions of RPs in the target area are segment-based, grid-based, and cube-based in the 1D, 2D, and 3D space, respectively. To make

the channels of these RPs approximately independent, we choose the spacing between the RPs as the average correlation distance, e.g., the spacing is set to 11 m, 21 m, and 45 m for UMi, UMa LOS, and UMa NLOS, respectively [6]. As such, each RP can be considered as the beginning of a channel segment.

Then we briefly introduce the generation of LSPs of these RPs. We consider the following eight LSPs: RMS-DS, SF, Ricean K-factor (KF), azimuth spread of departure (ASD), azimuth spread of arrival (ASA), elevation spread of departure (ESD), elevation spread of arrival (ESA), and cross-polarization ratio (XPR). As stochastic processes, the above eight LSPs of RPs are generated randomly by the SOS method based on the geographic positions of RPs and the statistical distribution functions drawn from field measurement data. Then the cluster powers, cluster delays, departure and arrival angles are also generated randomly by the SOS method according to the spatial positions of RPs, the empirical distribution functions, and the generated LSPs. Specific generation methods can refer to QuaDRiGa documents [21].

B. Calculation and Storage of Clusters Positions

To update the cluster delays and angles when the MT moves, the positions of the clusters involved in the NLOS propagations are required. We consider the multi-bounce model in which both the first-bounce scatterer (FBS) and last-bounce scatterer (LBS) are taken into account [21]. The NLOS propagation can be divided into three parts, as shown in Fig.3. Firstly, the ray emitted from the BS side reaches the FBS directly, then it propagates from the FBS to the LBS, and finally reaches the MT. As such, the departure angles are determined by the relative positions between the FBSs and BS, while the arrival angles are determined by the relative positions between the LBSs and MT.

To realize the spatial consistency in the target area, the scattering environment needs to be consistent. Since the RPs are evenly selected throughout the space, we assume the summation of clusters of each RP constitutes the overall scattering environment. The QuaDRiGa document [21] has resolved the calculation of the positions of the FBS and the LBS in the multi-bounce model using the cluster delays and angles. Based on this, we calculate the positions of clusters

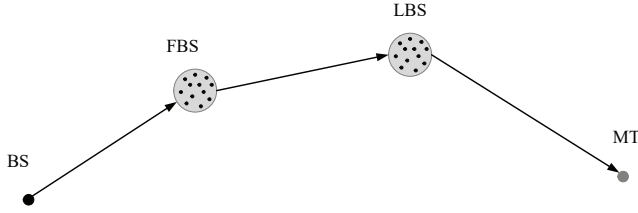


Fig. 3: Multi-bounce model.

of the RPs and store them in our database. By doing so, the overall scattering environment is determined and fixed.

C. Transition between RPs

To realize the spatial consistency at the cluster level in the entire space, we propose to generate the channel of the MT based on the transitions between the RPs. In the rest of this section, we first describe the RPs transition in the 1D space, based on which we then describe the RPs transition in the 2D or 3D space.

In the 1D space, the RPs are arranged with equal spacing in a straight line. We assume the channel of the MT is determined by the scattering environment of the most two neighboring RPs. When the MT moves from one RP to another RP, the clusters of the old RP's channel are gradually replaced by that of the new one, resulting in the transition of the channel. Specifically, we couple the clusters of the two RPs based on their RMS-DS and power. To keep the computational overhead low, the interval between adjacent RPs is divided into numbers of sub-intervals with each of them corresponding to the survival space of a pair of clusters. During each sub-interval, the power of the new cluster is positively correlated with the length of the MT movement in the sub-interval d , and the power of the old one is negatively correlated with the length d until the old one is replaced totally by the new one. To meet the above conditions, we assume that the power changes of the new and old clusters in the sub-interval are linear, and the function of power ramps is modeled as

$$\begin{aligned} w(d) &= \frac{d}{d_s}, \\ w_{\text{old}}(d) &= \sqrt{1 - w(d)}, \\ w_{\text{new}}(d) &= \sqrt{w(d)}, \end{aligned} \quad (4)$$

where $w_{\text{old}}(\cdot)$ represents the ramp function of the old cluster, $w_{\text{new}}(\cdot)$ represents the ramp function of the new cluster, and d_s is the length of the sub-interval. If the number of clusters in the two RPs is different, then the weakest clusters are ramped up or down over the interval individually without coupling.

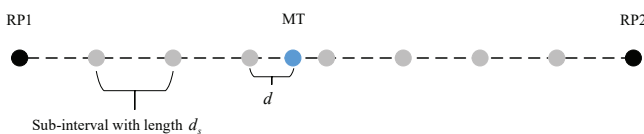


Fig. 4: Transition in the 1D space.

Fig. 4 shows the RPs transition in the 1D space. We assume that the number of clusters of RP1 and RP2 is equal and

denoted by N_p . Since each sub-interval between the RP1 and RP2 corresponds to a pair of clusters, the number of sub-intervals is also equal to N_p . We next describe how to model the appearance and disappearance of clusters when the MT moves between RP1 and RP2. We reorder the clusters of RP1 and RP2 and pair the clusters that have the same index. Let o_1 and o_2 be the sequences of an arrangement of the RP1's clusters' indices and the RP2's clusters' indices, respectively. The i th element in the sequences o_1 and o_2 are denoted by $o_1(i)$ and $o_2(i)$, respectively. When the MT is located in the n th sub-interval, the clusters of RP1 with indices from $o_1(1)$ to $o_1(n-1)$ are replaced by the clusters of RP2 with indices from $o_2(1)$ to $o_2(n-1)$, and the cluster of RP1 with index $o_1(n)$ is ramped down and the cluster of RP2 with index $o_2(n)$ is ramped up based on the distance d . Let the channel gains of the i th cluster of RP1 and RP2 are denoted by $\alpha_{i,1}$ and $\alpha_{i,2}$, respectively. For integers $i = 1, \dots, n-1$ and $j = n+1, \dots, N_p$, we calculate the channel gains of the m th MT in the n th sub-interval as

$$\begin{aligned} \alpha_{i,m} &= \alpha_{o_1(i),2}, \\ \alpha_{n,m} &= w_{\text{new}}(d) \cdot \alpha_{o_2(n),2}, \\ \alpha_{n+1,m} &= w_{\text{old}}(d) \cdot \alpha_{o_1(n),1}, \\ \alpha_{j+1,m} &= \alpha_{o_1(j),1}. \end{aligned} \quad (5)$$

The i th cluster powers of RP1 and RP2 are denoted by $p_{i,1}$ and $p_{i,2}$, respectively, and their sum powers are denoted by $P_1 = \sum_{i=1}^{N_p} p_{i,1}$ and $P_2 = \sum_{i=1}^{N_p} p_{i,2}$, respectively. The sum power of the MT with the moving distance of d in the n th sub-interval is given by

$$\begin{aligned} P'_n(o_1, o_2, d) &= \sum_{i=1}^{n-1} p_{o_2(i),2} + \sum_{i=n+1}^{N_p} p_{o_1(i),1} \\ &\quad + w_{\text{old}}^2(d) \cdot p_{o_1(n),1} + w_{\text{new}}^2(d) \cdot p_{o_2(n),2}. \end{aligned} \quad (6)$$

Then we illustrate how to determine the arrangements of o_1 and o_2 . Let the i th cluster delays of RP1 and RP2 denoted by $\tau_{i,1}$ and $\tau_{i,2}$, respectively. Then the RMS-DSs of RP1 and RP2 are calculated as

$$D_1 = \sqrt{\frac{\sum_{i=1}^{N_p} p_{i,1} \tau_{i,1}^2 - \left(\sum_{i=1}^{N_p} p_{i,1} \tau_{i,1} \right)^2}{P_1}} \quad (7)$$

and

$$D_2 = \sqrt{\frac{\sum_{i=1}^{N_p} p_{i,2} \tau_{i,2}^2 - \left(\sum_{i=1}^{N_p} p_{i,2} \tau_{i,2} \right)^2}{P_2}}, \quad (8)$$

respectively. The actual RMS-DS of MT at the end of the n th sub-interval is given in (9), shown at the top of next page, where $P'_n(o_1, o_2) \triangleq P'_n(o_1, o_2, d_s)$. As we have illustrated in Section II-B, RMS-DS is an important characteristic of spatial consistency, thus we should dedicate to the RMS-DS to determine the arrangements of o_1 and o_2 . The actual RMS-DS variation curve calculated by the SSPs may fluctuate in a stochastic way during the transition between the RPs. For

$$D'_n(o_1, o_2) = \sqrt{\frac{\sum_{i=1}^n p_{o_2(i),2} \tau_{o_2(i),2}^2 + \sum_{i=n+1}^{N_p} p_{o_1(i),1} \tau_{o_1(i),1}^2 - \left(\sum_{i=1}^n p_{o_2(i),2} \tau_{o_2(i),2} + \sum_{i=n+1}^{N_p} p_{o_1(i),1} \tau_{o_1(i),1} \right)^2}{P'_n(o_1, o_2)}} \quad (9)$$

example, the RMS-DS will decrease if a strong cluster with a large delay ramps down and its coupled weak cluster with a small delay ramps up, and vice versa. According to Theorem 1, the true RMS-DS varies continuously in the space, and we can assume the target RMS-DS changes in proportion to the distance. To minimize the impact of the RPs transition on RMS-DS fluctuations, the optimal o_1 and o_2 can be obtained by solving the following optimization problem

$$\arg \min_{o_1, o_2} \sum_{n=1}^{N_p} \left(D'_n(o_1, o_2) - \tilde{D}_n \right)^2 \cdot b(o_1, o_2), \quad (10)$$

where $\tilde{D}_n = D_1 + \frac{n}{N_p} (D_2 - D_1)$ denotes the target RMS-DS in the n th sub-interval, and $b(o_1, o_2)$ is the penalty of channel power introduced by [7], [10]

$$b(o_1, o_2) = \max_{n=1, \dots, N_p} \left(\frac{P'_n(o_1, o_2, d_s)}{P_1 + \frac{n}{N_p} (P_2 - P_1)} \right). \quad (11)$$

The basic idea behind the optimization problem (10) is to minimize the cost between the target RMS-DSs $\tilde{D}_n, n = 1, 2, \dots, N_p$ and the optimized RMS-DSs $D'_n(o_1, o_2), n = 1, 2, \dots, N_p$ in all sub-intervals by searching the couple of the clusters.³

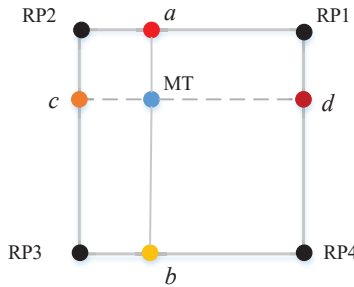


Fig. 5: Transition in the 2D space.

In the 2D space, the evenly spaced RPs and the lines connecting them divide the target area into individual grids. To ensure the rationality of the transition in the 2D space, we propose the following three constraints:

- 1) When the MT falls in the grid area as shown in Fig. 5, the scattering environment around the MT is consistent with the scattering environment around the four vertices.
- 2) The transition can reflect the continuity of RMS-DS change in the space.
- 3) The result of the transition is unique.

With the consideration of the first two constraints, we transfer the transition in the 2D space into a two-step transition

³The typical solution of the optimization problem (10) refers to the heuristic iteration method in [10], [21].

in the 1D space. In the first step, the position of the MT is projected on the lines connecting the vertices RP1, RP2, and the vertices RP3, RP4, respectively. Fig. 5 illustrates this projection method. The projection points are denoted as a and b , respectively. Using the transition method in the 1D space, we calculate the cluster powers and phases of the point a with the vertices RP1 and RP2, and the cluster powers and phases of the point b with the vertices RP3 and RP4. In the second step, since the MT is in the line connecting a and b , we then calculate the cluster powers and phases of the MT with a and b as the RPs using the transition method in the 1D space.

To prove the uniqueness of this method, we consider another way of projection: the position of the MT is projected on the lines connecting the vertices RP2, RP3 and the vertices RP1, RP4, with the projection points denoted by c and d . Let D_1, D_2, D_3, D_4 denote the RMS-DS of RP1, RP2, RP3, RP4 respectively. In the first way of projection, the RMS-DS of the point a is approximated based on the transition in the 1D space, given by

$$D_a = D_2 + k(D_1 - D_2) = k \cdot D_1 + (1 - k) \cdot D_2, \quad (12)$$

where

$$k = \frac{|x_m - x_3|}{d_c}, \quad (13)$$

where x_3 and x_m are the x -coordinates of the RP3 and the m th MT, respectively, and d_c is the distance between two adjacent RPs. Similarly, the RMS-DS of the point b is given by

$$D_b = k \cdot D_4 + (1 - k) \cdot D_3. \quad (14)$$

Then we approximate the RMS-DS of the MT as

$$D_m = l \cdot D_a + (1 - l) \cdot D_b, \quad (15)$$

where

$$l = \frac{|y_m - y_3|}{d_c}, \quad (16)$$

where y_3 and y_m are the y -coordinates of the RP3 and the m th MT, respectively.

In the second way of projection, the RMS-DSs of the point c and d are approximated as

$$D_c = l \cdot D_2 + (1 - l) \cdot D_3, \quad (17)$$

and

$$D_d = l \cdot D_1 + (1 - l) \cdot D_4, \quad (18)$$

respectively. Then the RMS-DS of the m th MT is approximated as

$$D'_m = k \cdot D_d + (1 - k) \cdot D_c. \quad (19)$$

Define the weight vectors as

$$\mathbf{k} = [k, 1 - k]^T, \quad (20)$$

$$\mathbf{1} = [l, 1 - l]^T, \quad (21)$$

and the RMS-DS matrix as

$$\mathbf{D} = \begin{bmatrix} D_1 & D_3 \\ D_2 & D_4 \end{bmatrix}. \quad (22)$$

For the sake of clarity, we represent the expressions in (15) and (19) in vector form, given as

$$D_m = \mathbf{1}^T \cdot [D_a, D_b]^T = \mathbf{1}^T \mathbf{D}^T \mathbf{k}, \quad (23)$$

and

$$D'_m = \mathbf{k}^T \cdot [D_d, D_c]^T = \mathbf{k}^T \mathbf{D} \mathbf{1}, \quad (24)$$

respectively. Hence, we have

$$D'_m = \mathbf{k}^T \mathbf{D} \mathbf{1} = (\mathbf{1}^T \mathbf{D}^T \mathbf{k})^T = D_m. \quad (25)$$

So the transition results obtained by the two projection methods are the same. The third constrain is satisfied.

Hereafter we consider the RMS-DS variation in two special cases: the MT moves from the inner area of the grid to the edge of the grid; the MT moves from the inner area of the grid to the vertices of the grid. In the first case, let the MT approaches the point b that falls on the edge of the grid. From (15) and (16), we have

$$\lim_{y_m \rightarrow y_3} D_m = D_b. \quad (26)$$

Therefore, the RMS-DS changes continuously when the MT moves from the inner area of the grid to the edge of the grid. Further, when the MT falls on edge of the grid, its RMS-DS is totally determined by the nearest two RPs. In this case, the transition in the 2D space is consistent with that in the 1D space. In the second case, let the MT approaches the RP3. From (12), (14) and (15), we have

$$\lim_{x_m \rightarrow x_3, y_m \rightarrow y_3} D_m = D_3. \quad (27)$$

Thus, the RMS-DS also changes continuously when the MT moves from the inner area of the grid to the vertices of the grid. The RMS-DS of the MT is consistent with the RMS-DS of the RPs when the MT coincides with the RPs.

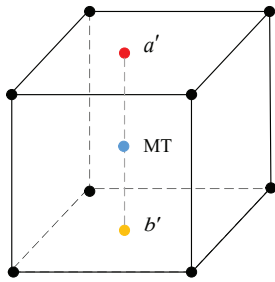


Fig. 6: Transition in the 3D space.

In the 3D space, the situation is more complicated. The evenly spaced RPs and the lines connecting them divide the target area into individual cubes, as described in Fig. 6. When the MT falls in the cube area, we assume that the channel coefficients of the MT are only related to the scattering environment around the eight vertices and their channel coefficients. Inspired by the transition in the 2D space,

we further transfer the transition in the 3D space into a two-step transition using the transition in the 1D and 2D space. The MT is first projected onto the upper and lower surfaces of the cube, and the projection points are denoted as a' and b' , as shown in Fig. 6. Then based on the transition in the 2D space, we calculate the cluster powers and phases at a' and b' . Finally, the cluster powers and phases of the MT are calculated with a' and b' as the RPs using the transition in the 1D space. The three constraints are also satisfied for transition in the 3D space, of which the discussion process is similar to that in the 2D space and hence we omit it.

D. Update of Cluster Delays and Angles

After realizing spatial evolution of clusters through the transitions between RPs proposed in section III-C, the cluster powers, phases, and the corresponding FBSs and LBSs are available for the MT. Let the position of the m th MT's receive antenna be \mathbf{a}_m and the center position of the b th BS's transmit antenna be \mathbf{a}_b . To further realize the spatial evolutions of LSPs and SSPs, we update the delays and angles for each cluster of the MT based on geographic calculation by using the positions calculated in Section III-B. The i th cluster delay of the m th MT is updated as

$$\tau_{i,m} = \frac{\|\mathbf{a}_b - \mathbf{a}_{i,s,1}\| + \|\mathbf{a}_{i,s,1} - \mathbf{a}_{i,s,2}\| + \|\mathbf{a}_m - \mathbf{a}_{i,s,2}\|}{c}, \quad (28)$$

where c is the light speed, $\mathbf{a}_{i,s,1}$ and $\mathbf{a}_{i,s,2}$ are the positions of FBS and LBS of the i th cluster, respectively, and $\|\cdot\|$ is the Euclidean norm. Let $[\cdot]_i$ represent the i th element of a vector. The elevation and azimuth angles between the FBS of the i th cluster and the b th BS's transmit antenna are updated as

$$\theta_{i,b} = \arccos \left(\frac{[\mathbf{a}_{i,s,1} - \mathbf{a}_b]_3}{\|\mathbf{a}_{i,s,1} - \mathbf{a}_b\|} \right), \quad (29)$$

$$\varphi_{i,b} = \arctan \left(\frac{[\mathbf{a}_{i,s,1} - \mathbf{a}_b]_2}{[\mathbf{a}_{i,s,1} - \mathbf{a}_b]_1} \right), \quad (30)$$

respectively. Similarly, the elevation and azimuth angles between the LBS of the i th cluster and the m th MT's transmit antenna are updated as

$$\theta_{i,m} = \arccos \left(\frac{[\mathbf{a}_{i,s,2} - \mathbf{a}_m]_3}{\|\mathbf{a}_{i,s,2} - \mathbf{a}_m\|} \right), \quad (31)$$

$$\varphi_{i,m} = \arctan \left(\frac{[\mathbf{a}_{i,s,2} - \mathbf{a}_m]_2}{[\mathbf{a}_{i,s,2} - \mathbf{a}_m]_1} \right). \quad (32)$$

IV. SIMULATION RESULTS

In this section, we evaluate the performance of the spatial consistency of the channel simulator with the proposed RPs transition method. We first provide three performance metrics from different levels to evaluate spatial consistency. Then, we illustrate the settings of the simulation. Finally, we compare the performance of spatial consistency between the channel simulator with RPs transition method and the original QuaDRiGa using the simulation results.

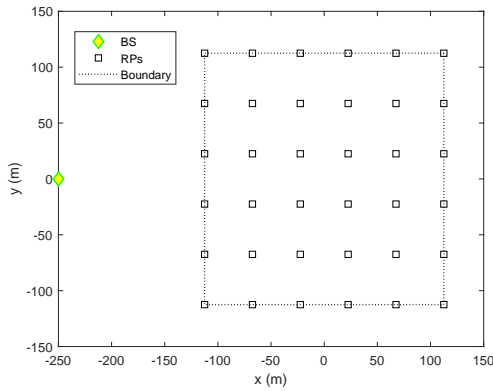


Fig. 7: BS and RPs in the target area.

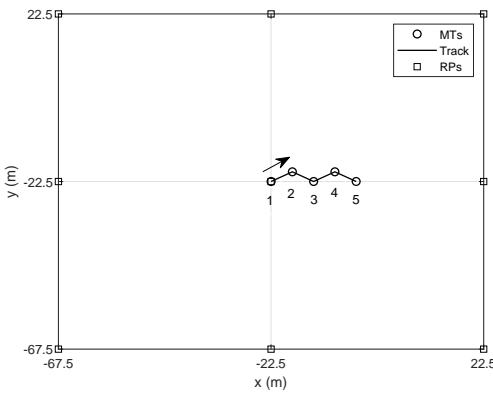


Fig. 8: MTs in the track.

A. Performance Metrics

1) *LSP level*: The evolution of LSPs along with the MTs' positions. Two geographically neighboring MTs will share related LSPs due to the similar scattering environment. As the LSPs, RMS-DS and AS are the second moments of time delay and angle, respectively [31]. It is worth noting that there are four ASs, including ASD, ASA, ESD, and ESA. Without loss of generality, we only pay attention to the evolution of ASD along with the MTs' positions.

2) *SSP level*: The evolution of SSPs along with the MTs' positions. The channel PDP and power angle spectrum (PAS) give the power intensity of a multipath channel as a function of time delay and angle, respectively [28]. On the one hand, for closely spaced MTs, their surrounding scattering environment maintains similarity, leading to related PDP and PAS. On the other hand, we can easily observe the birth and death of clusters along with the MTs' positions from the PDP and PAS. Therefore, PDP and PAS are both reasonable metrics of spatial consistency at the SSP level. Note that the cluster angles include the azimuth angle of departure (AOD), the elevation angle of departure (EOD), the azimuth angle of arrival (AOA), and the elevation angle of arrival (EOA). Without loss of generality, we only focus on the PAS with respect to the AOD.

3) *Cluster level*: The evolution of cluster positions along with the MTs' positions. According to the WSS conditions, the

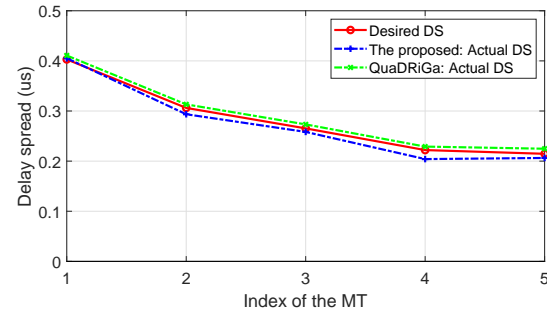


Fig. 9: RMS-DS evolution along with the MTs' positions.

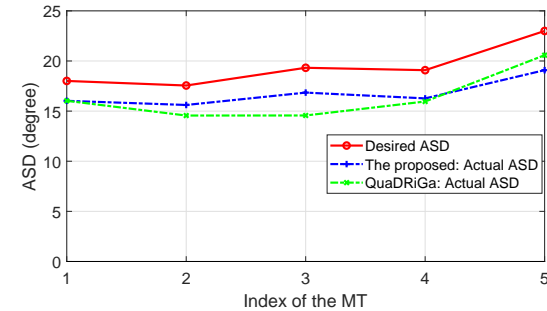


Fig. 10: ASD evolution along with the MTs' positions.

cluster positions are nearly fixed for closely spatial positions [21]. In other words, for two closely spaced MTs, cluster positions are almost the same with the birth and death of a small number of clusters. Therefore, the spatial evolution of cluster positions is also an important metric for spatial consistency.

B. Simulation Setup

We consider the 3GPP UMa NLOS scenario where the carrier frequency is set to 2 GHz. We set the average correlation distance $d_c = 45$ m according to the 3GPP NR channel model [6], and the spacing between the RPs equals to d_c as illustrated in Section III-A. We consider a 225×225 m² target area with its center located at the origin (0, 0) m, of which the boundary is shown in Fig. 7 by the dotted line. The BS is equipped with a uniform planar array (UPA) at (-250, 0) m, comprising 16 antennas in each row and 4 antennas in each column. The antenna plane is perpendicular to the ground and faces the target area. The MT is equipped with an omni-directional antenna and moves within the target area. The heights of the BS's antenna array and the MT's antenna are set to 25 m and 1.5 m, respectively, as recommended in the 3GPP channel models [5], [6]. The RPs are evenly spaced in the target area. In Fig. 7, we present the BS and RPs by the green diamond and black squares, respectively.

We preset a track presented by the black line in the target area to observe the spatial evolutions of LSPs, SSPs, and cluster positions, as shown in Fig. 8. We place five MTs presented by the black circles at five positions of the track, and the direction of the track changes 120° once reaching a new MT. We mark the five positions along the direction of the

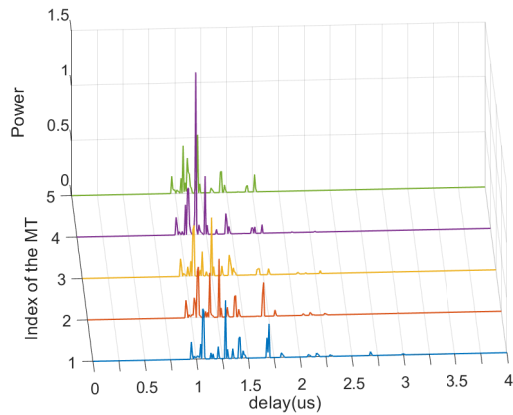


Fig. 11: PDP evolution of the channel simulator with RPs transition method along with the MTs' positions.

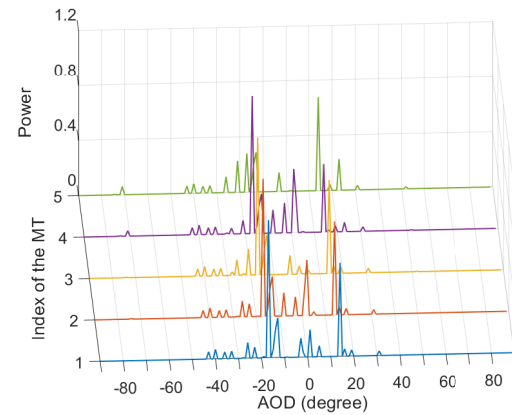


Fig. 13: PAS evolution of the channel simulator with RPs transition method along with the MTs' positions.

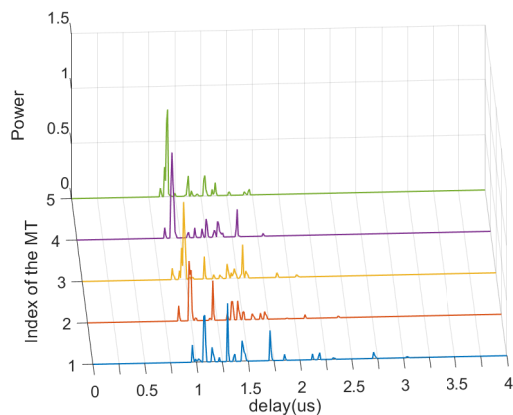


Fig. 12: PDP evolution of the original QuaDRiGa along with the MTs' positions.

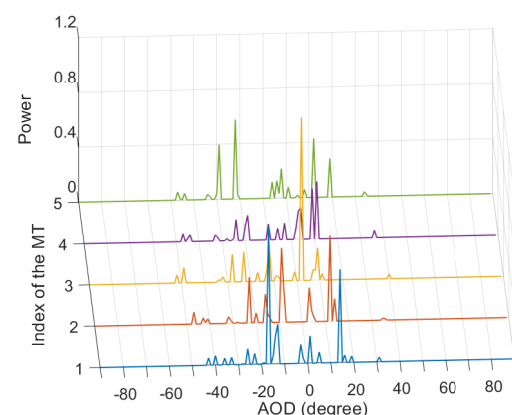


Fig. 14: PAS evolution of the original QuaDRiGa along with the MTs' positions.

track using the indices from 1 to 5. The distance between two adjacent MTs is five meters in the track. Note that the MTs can be placed at arbitrary positions of the target areas, which are not limited to the above track.

C. Simulation Results

Fig. 9 and Fig. 10 present the performance comparisons of spatial consistency at the LSP level. The RMS-DS evolutions with the MTs' positions are shown in Fig. 9. We can observe that the RMS-DS spatial evolution curves of both the QuaDRiGa and the channel simulator with the proposed RPs transition method can fit with the desired RMS-DS curve well. The superior fitting results of the simulator with RPs transition method benefit from the optimization of RMS-DS in equation (10). Fig. 10 shows ASD evolutions with the MTs' positions. Although our proposed method does not specifically optimize for AS, the simulator with RPs transition method can still achieve similar performance with the original QuaDRiGa in terms of the spatial consistency of ASD. Note that 'Desired LSP' in the legend is generated by the SOS method as the input of the SSP model, while 'Actual LSP' is calculated according to the actual generated SSPs.

The PDP evolution of the channel simulator with RPs transition method along with the MTs' positions is demonstrated

in Fig. 11. The difference between the PDPs at two adjacent positions, e.g., the 1st position and 2nd position, is small, while the PDPs at the 1st and 5th positions appear considerable difference. The birth and death of the clusters can be roughly observed through the appearance and disappearance of the power spikes on the delay axis in the movement. Fig. 12 shows the PDP evolution of the original QuaDRiGa along with the MTs' positions. On the contrary, even if the positions of two MT are adjacent, the PDPs at such two positions appear obviously different. Specifically, for the 1st position and 2nd position, the shift of most power spikes on the delay axis implies that the positions of the majority of clusters are changed, which violates the WSS conditions over a short distance.

Fig. 13 presents the PAS evolution of the channel simulator with RPs transition method along with the MTs' positions. From the 1st position to the 5th position, the PAS varies gradually and the appearance and disappearance of the power spikes on the AOD axis occur, indicating the birth and death of the clusters. Fig. 14 presents the PAS evolution of the original QuaDRiGa along with the MTs' positions. We can observe that the variation of the PAS over space is significant so that a large number of clusters are born and died even for two adjacent MTs.

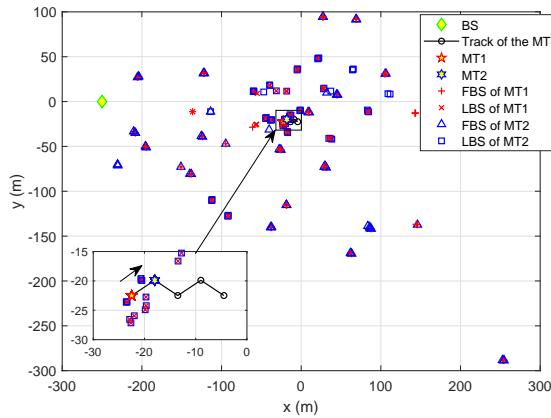


Fig. 15: The evolution of cluster positions of the channel simulator with RPs transition method from MT1 to MT2.

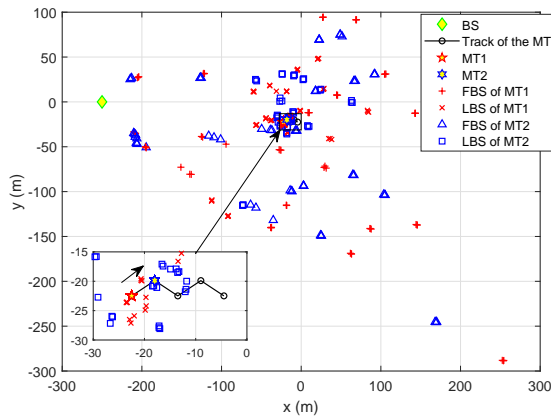


Fig. 16: The evolution of cluster positions of the original QuaDRiGa from MT1 to MT2.

To further demonstrate the spatial consistency at the cluster level, we plot the evolutions of cluster positions of the channel simulator with the proposed RPs transition method and the original QuaDRiGa from MT1 to MT2, as shown in Fig. 15 and Fig. 16, respectively. MT1 and MT2 are presented by the red pentagon and blue hexagon, respectively. To distinguish different kinds of scatterers, we present the FBSs of MT1, the LBSs of MT1, the FBSs of MT2, and the LBSs of MT2 by the red pluses, red crosses, blue triangles, and blue squares, respectively. In Fig. 15, we can observe that most scatterers of MT1 overlap those of MT2 along with the birth and death of a small number of clusters. In contrast, there is little overlap between the scatterers of MT1 and MT2 even though the distance between two MTs is very short (only 5 m), as shown in Fig. 16. Sometimes, the distance between the cluster positions of two adjacent MTs is several times or even tens of times longer than that between two MTs, which violates the WSS conditions, i.e., the cluster positions are nearly fixed for closely neighboring spatial positions. In addition, the spatial evolution of cluster positions can well explain the simulation results of the spatial evolutions of PDP and PAS.

From the perspective of the generation order of the MT's channel parameters, the existing GSCM-based channel simu-

lators' order is LSPs, SSPs, and clusters, which is opposite to the practical physical generation order (i.e., the clusters determine the SSPs which further determine the LSPs). From the simulation results of the QuaDRiGa, we can observe that the small changes of SSPs such as cluster delay and angles over space may contribute to the large and abrupt changes of cluster positions. Although the existing GSCM-based channel simulators try to realize the continuous changes of LSPs and SSPs over space, the cluster positions calculated by the SSPs according to the multi-bounce model [21] may appear considerably different even over a short distance between two MTs, as shown in Fig. 16. By comparison, the generation order of the MT's channel parameters in our proposed RPs transition method is consistent with the practical physical generation order. According to the simulation results of the channel simulator with RPs transition method, the small changes of clusters can correspond to the small and continuous changes of LSPs and SSPs. Hence, the channel simulator with RPs transition method can ensure that the cluster appearance and disappearance satisfy the WSS conditions even for closely neighboring spatial positions as shown in Fig. 15, resulting in the spatial consistency of LSPs and SSPs based on geographic calculation. Therefore, the channel simulator with the proposed RPs transition method can achieve better performance of spatial consistency than the existing ones at the SSP and cluster levels.

V. CONCLUSION

In this paper, we proposed the RPs transition method to improve the cluster-level spatial consistency of channel simulator in the entire 2D or 3D space. We first introduced the concept of correlation distance and derived the continuity of the RMS-DS in the space. Then we proposed to choose the RPs according to the correlation distance and generate their channels stochastically based on the SOS method. Next, we proposed the RPs transition method based on the RMS-DS continuity to generate the MT's channel deterministically, which realizes the spatial consistency of clusters. Finally, the cluster delays and angles were further updated based on geographic calculation to realize the spatial consistency of LSPs and SSPs. The simulation results demonstrated that the channel simulator with RPs transition method could achieve spatial consistency at the LSP, SSP, and cluster levels over the entire space.

APPENDIX A PROOF OF THEOREM 1

We assume the positions of the b th BS and m th MT are $\mathbf{a}_b = (x_b, y_b)$ and $\mathbf{a}_m = (x_m, y_m)$, respectively. The distance between them is given as

$$d_m = \|\mathbf{a}_m - \mathbf{a}_b\| = \sqrt{(x_m - x_b)^2 + (y_m - y_b)^2}. \quad (33)$$

Given the propagation path shown in Fig. 1, the signal propagates from the BS to the scatterer and then reaches the MT. Let the distance and angle from the MT to the s th scatterer

be r_s and θ_s , respectively. The distance from the scatterer to the b th BS is calculated as

$$r_b = \sqrt{d_m^2 + r_s^2 - 2r_s d_m \cos(\theta_s)}. \quad (34)$$

Then the delay of the propagation path is calculated as

$$\tau = \frac{r_s + r_b}{c}, \quad (35)$$

where c is the light speed.

We then calculate the probability density function (PDF) of the distribution of τ . Let $A(\tau, d_m)$ denotes the area of the overlapping region of the ellipse with the scattering circle, as shown in Fig. 17. The semi-major axis of the ellipse is $a = \frac{\tau c}{2}$ with the BS and the MT as its focus. According to [27], $A(\tau, d_m)$ is calculated as

$$\begin{aligned} A(\tau, d_m) &= R^2 \alpha + \frac{d_m^2 - \tau^2 c^2}{4} \cdot \left(\frac{-\pi \tau c}{\sqrt{\tau^2 c^2 - d_m^2}} + \frac{d \sin(\alpha)}{\tau c - d_m \cos(\alpha)} \right. \\ &\quad \left. + \frac{2\tau c}{\sqrt{\tau^2 c^2 - d_m^2}} \cdot \arctan \left(\frac{\sqrt{\tau^2 c^2 - d_m^2} \tan(\frac{\alpha}{2})}{\tau c - d_m} \right) \right), \\ \frac{d_m}{c} \leq \tau \leq \frac{d_m + 2R}{c}, d_m > 0, \end{aligned} \quad (36)$$

where α is the angle from the MT to the intersection of the circle with ellipse. By substituting α for θ_s in (34) and R for r_s in (35), and squaring both sides of (35), we solve that

$$\alpha = \arccos \left(\frac{d_m^2 + 2R\tau c - \tau^2 c^2}{2Rd_m} \right). \quad (37)$$

Because the scatterers are uniformly distributed in the scattering circle, the cumulative density function (CDF) of τ can be calculated as the divisor of $A(\tau, d_m)$ and the area of scattering circle, given by

$$F(\tau; d_m) = \frac{A(\tau, d_m)}{\pi R^2}. \quad (38)$$

By taking the derivative of (38) with respect to τ , the PDF of τ is calculated as

$$f_\tau(\tau; d_m) = \frac{1}{\pi R^2} \frac{d}{d\tau} A(\tau, d_m), \quad \frac{d_m}{c} \leq \tau \leq \frac{d_m + 2R}{c}. \quad (39)$$

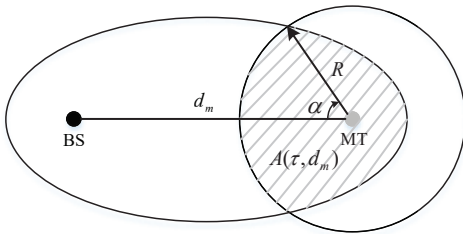


Fig. 17: PDF calculation of the delay in circular scattering model.

Assume that the power of all subpaths is equal, and the total power of subpaths is normalized to 1. Then the subpath power is given by $p_n = \frac{1}{N_s}$ for $n = 1, 2, \dots, N_s$, where N_s

is the number of subpaths. We divide the delay domain into many intervals with a spacing of $\Delta\tau$. Given a non-negative integer i , the probability of subpath delay τ which lies in the i th interval $[i\Delta\tau, (i+1)\Delta\tau]$ can be approximated by

$$\rho_i \approx f_\tau(i\Delta\tau; d_m) \cdot \Delta\tau. \quad (40)$$

When the number of subpaths N_s is quite large, according to the law of large numbers, the number of subpaths corresponding to the i th delay interval $[i\Delta\tau, (i+1)\Delta\tau]$ is approximated by

$$\Lambda_i \approx N_s \cdot \rho_i, \quad i = 0, 1, \dots. \quad (41)$$

Let $\Delta\tau \rightarrow 0$, the RMS-DS with the distance between the BS and the MT equaling to d_m is calculated as

$$\begin{aligned} D(d_m) &= \sqrt{\sum_{n=1}^{N_s} p_n \cdot \tau_n^2 - \left(\sum_{n=1}^{N_s} p_n \cdot \tau_n \right)^2} \\ &= \sqrt{\lim_{\Delta\tau \rightarrow 0} \sum_{i=1}^{\infty} \frac{1}{N_s} (i\Delta\tau)^2 \Lambda_i - \left(\lim_{\Delta\tau \rightarrow 0} \sum_{i=1}^{\infty} \frac{1}{N_s} i\Delta\tau \Lambda_i \right)^2} \\ &= \sqrt{\int_{\frac{d_m}{c}}^{\frac{d_m+2R}{c}} \tau^2 f_\tau(\tau; d_m) d\tau - \left(\int_{\frac{d_m}{c}}^{\frac{d_m+2R}{c}} \tau f_\tau(\tau; d_m) d\tau \right)^2}. \end{aligned} \quad (42)$$

From (42), the calculation of RMS-DS comes to the calculation of the variance of τ . Using partial integration, (42) can be further rewritten as

$$D(d_m) = \sqrt{\psi_\tau(d_m) - m_\tau^2(d_m)}, \quad (43)$$

where

$$\psi_\tau(d_m) = \frac{(d_m + 2R)^2}{c^2} - 2 \int_{\frac{d_m}{c}}^{\frac{d_m+2R}{c}} \frac{A(\tau, d_m)}{\pi R^2} \tau d\tau, \quad d_m > 0, \quad (44)$$

$$m_\tau(d_m) = \frac{d_m + 2R}{c} - \int_{\frac{d_m}{c}}^{\frac{d_m+2R}{c}} \frac{A(\tau, d_m)}{\pi R^2} d\tau, \quad d_m > 0. \quad (45)$$

The continuity theorem illustrates that:

- If functions f and g are continuous at x_0 , then functions $f + g$, $f - g$, $f \cdot g$, and $\frac{f}{g}(g(x_0) \neq 0)$ are also continuous at x_0 .
- If function $f(u)$ is continuous at point $u = u_0$ and function $u = g(x)$ is continuous at point $x = x_0$ and $u_0 = g(x_0)$, then the composite function $y = f(g(x))$ is continuous at point $x = x_0$.

According to the continuity theorem, $A(\tau, d_m)$ in (36) is continuous in the function definition domain $\frac{d_m}{c} \leq \tau \leq \frac{d_m+2R}{c}$, $d_m > 0$. Further, we have $\forall d_0 \in (0, +\infty)$,

$$\begin{aligned} \lim_{d_m \rightarrow d_0} \psi_\tau(d_m) &= \frac{(d_0 + 2R)^2}{c^2} - 2 \int_{\frac{d_0}{c}}^{\frac{d_0+2R}{c}} \frac{A(\tau, d_0)}{\pi R^2} \tau d\tau \\ &= \psi_\tau(d_0), \end{aligned} \quad (46)$$

and $\forall d_0 \in (0, +\infty)$,

$$\lim_{d_m \rightarrow d_0} m_\tau(d_m) = \frac{d_0 + 2R}{c} - \int_{\frac{d_0}{c}}^{\frac{d_0 + 2R}{c}} \frac{A(\tau, d_0)}{\pi R^2} d\tau \quad (47)$$

$$= m_\tau(d_0).$$

Therefore $\psi_\tau(d_m)$ and $m_\tau(d_m)$ are continuous in the function definition domain $d > 0$. From (43), we derive

$$\lim_{d_m \rightarrow d_0} D(d_m) = \sqrt{\lim_{d_m \rightarrow d_0} \psi_\tau(d_m) - \lim_{d_m \rightarrow d_0} m_\tau^2(d_m)} \quad (48)$$

$$= D(d_0),$$

which means $D(d_m)$ is continuous when $d_m > 0$. According to the expression of d_m in (33), the RMS-DS with respect to the position \mathbf{a}_m is given by

$$D(\mathbf{a}_m) = D(d_m)|_{d_m = \|\mathbf{a}_m - \mathbf{a}_b\|}. \quad (49)$$

Because the function d_m is continuous with respect to \mathbf{a}_m , $D(\mathbf{a}_m)$ is also continuous with respect to \mathbf{a}_m in the target space. Given an arbitrary position \mathbf{a}_0 in the target space and $\|\mathbf{a}_0 - \mathbf{a}_b\| = d_0$, by substituting (49) into (48), we obtain (1). This completes the proof.

ACKNOWLEDGEMENT

We thank Xinyue Chen from Southeast University, China for the insightful discussion that greatly assisted this work.

REFERENCES

- [1] C. Wang, J. Bian, J. Sun, W. Zhang, and M. Zhang, "A survey of 5G channel measurements and models," *IEEE Commun. Surveys Tuts.*, vol. 20, no. 4, pp. 3142–3168, Aug. 2018.
- [2] C.-X. Wang, J. Huang, H. Wang, X. Gao, X. You, and Y. Hao, "6G wireless channel measurements and models: Trends and challenges," *IEEE Veh. Technol. Mag.*, vol. 15, no. 4, pp. 22–32, 2020.
- [3] M. Mbeutcha, W. Fan, J. Hejlsbæck, and G. F. Pedersen, "Evaluation of massive MIMO systems using time-reversal beamforming technique," Valencia, Spain, Sep. 2016, pp. 1–6.
- [4] 3GPP TR 25.996 v16.0.0, "Spatial channel model for Multiple Input Multiple Output (MIMO) simulations, Version 16.0.0," Tech. Rep., 2020.
- [5] 3GPP TR 36.873 v12.7.0, "Study on 3D channel model for LTE, Version 12.7.0," Tech. Rep., 2017.
- [6] 3GPP TR 38.901 v16.1.0, "Study on channel model for frequencies from 0.5 to 100 GHz," Tech. Rep., 2019.
- [7] Y. J. Bultitude, and T. Rautiaainen, "IST-4-027756 WINNER II D1.1.2 V1.2: WINNER II Channel Models," Tech. Rep., 2007. [Online]. Available: <https://www.ist-winner.org>
- [8] V. Nurmela, A. Karttunen, A. Roivainen, L. Raschkowski, V. Hovinen, J. Y. EB, N. Omaki, K. Kusume, A. Hekkala, R. Weiler *et al.*, "ICT-317669-MIETS/D1.4: METIS channel models," Tech. Rep., 2015.
- [9] M. Peter, K. Haneda, S. Nguyen, A. Karttunen, and J. Järveläinen, "H2020-ICT-671650-mmMAGIC/D2.2: Measurement results and final mmMAGIC channel models," Tech. Rep., 2017.
- [10] S. Jaeckel, L. Raschkowski, K. Borner, and L. Thiele, "QuaDRiGa: A 3-D multi-cell channel model with time evolution for enabling virtual field trials," *IEEE Trans. Antennas Propag.*, vol. 62, no. 6, pp. 3242–3256, Jun. 2014.
- [11] L. Liu, C. Oestges, J. Poutanen, K. Haneda, P. Vainikainen, F. Quitin, F. Tufvesson, and P. D. Doncker, "The COST 2100 MIMO channel model," *IEEE Wireless Commun.*, vol. 19, no. 6, pp. 92–99, Dec. 2012.
- [12] R. Verdone and A. Zanella, *Pervasive mobile and ambient wireless communications: COST action 2100*. Springer, 2012.
- [13] Y. Wang, Z. Shi, L. Huang, Z. Yu, and C. Cao, "An extension of spatial channel model with spatial consistency," in *Proc. IEEE VTC-Fall*, Montreal, Canada, Sep. 2016, pp. 1–5.
- [14] S. Ju and T. S. Rappaport, "Simulating motion - Incorporating spatial consistency into NYUSIM channel model," in *Proc. IEEE VTC-Fall*, Chicago, USA, Aug. 2018, pp. 1–6.

- [15] F. Ademaj, M. K. Mueller, S. Schwarz, and M. Rupp, "Modeling of spatially correlated geometry-based stochastic channels," in *Proc. IEEE VTC-Fall*, Toronto, Canada, Sep. 2017, pp. 1–6.
- [16] F. Ademaj, S. Schwarz, K. Guan, and M. Rupp, "Ray-tracing based validation of spatial consistency for geometry-based stochastic channels," in *Proc. IEEE VTC-Fall*, Chicago, USA, Aug. 2018, pp. 1–5.
- [17] M. Patzold, U. Killat, and F. Laue, "A deterministic digital simulation model for Suzuki processes with application to a shadowed rayleigh land mobile radio channel," *IEEE Trans. Veh. Technol.*, vol. 45, no. 2, pp. 318–331, May 1996.
- [18] X. Cai and G. B. Giannakis, "A two-dimensional channel simulation model for shadowing processes," *IEEE Trans. Veh. Technol.*, vol. 52, no. 6, pp. 1558–1567, 2003.
- [19] A. A. Saleh and R. Valenzuela, "A statistical model for indoor multipath propagation," *IEEE J. Sel. Areas Commun.*, vol. 5, no. 2, pp. 128–137, Feb. 1987.
- [20] S. Jaeckel, L. Raschkowski, F. Burkhardt, and L. Thiele, "Efficient sum-of-sinusoids-based spatial consistency for the 3GPP new-radio channel model," in *Proc. IEEE GC Wkshps*, Abu Dhabi, UAE, 2018, pp. 1–7.
- [21] S. Jaeckel, L. Raschkowski, K. Börner, L. Thiele, F. Burkhardt, and E. Eberlein, "Quadriga-quasi deterministic radio channel generator, user manual and documentation," Fraunhofer Heinrich Hertz Institute, Tech. Rep. v2.6.1, 2021.
- [22] X. Sun, X. Gao, G. Y. Li, and W. Han, "Single-site localization based on a new type of fingerprint for massive MIMO-OFDM systems," *IEEE Trans. Veh. Technol.*, vol. 67, no. 7, pp. 6134–6145, Jul. 2018.
- [23] K. N. R. S. V. Prasad, E. Hossain, and V. K. Bhargava, "Machine learning methods for RSS-based user positioning in distributed massive MIMO," *IEEE Trans. Wireless Commun.*, vol. 17, no. 12, pp. 8402–8417, Dec. 2018.
- [24] N. Garcia, H. Wymeersch, E. G. Larsson, A. M. Haimovich, and M. Coulon, "Direct localization for massive MIMO," *IEEE Trans. Signal Process.*, vol. 65, no. 10, pp. 2475–2487, May. 2017.
- [25] M. Arnold, S. Dörner, S. Cammerer, and S. Ten Brink, "On deep learning-based massive MIMO indoor user localization," in *Proc. IEEE SPAWC*, Kalamata, Greece, Jun. 2018, pp. 1–5.
- [26] P. Petrus, J. H. Reed, and T. S. Rappaport, "Geometrically based statistical channel model for macrocellular mobile environments," in *Proc. IEEE GLOBECOM*, London, UK, Nov. 1996, pp. 1197–1201.
- [27] R. B. Ertel and J. H. Reed, "Angle and time of arrival statistics for circular and elliptical scattering models," *IEEE J. Sel. Areas Commun.*, vol. 17, no. 11, pp. 1829–1840, Nov. 1999.
- [28] A. Goldsmith, *Wireless Communications*. Cambridge University Press, 2005.
- [29] S. Wu, C. Wang, e. M. Aggoune, M. M. Alwakeel, and Y. He, "A non-stationary 3-D wideband twin-cluster model for 5G massive MIMO channels," *IEEE J. Sel. Areas Commun.*, vol. 32, no. 6, pp. 1207–1218, Jun. 2014.
- [30] S. Wu, C. Wang, e. M. Aggoune, M. M. Alwakeel, and X. You, "A general 3-D non-stationary 5G wireless channel model," *IEEE Trans. Commun.*, vol. 66, no. 7, pp. 3065–3078, Jul. 2018.
- [31] D. Baum *et al.*, "IST-2003-507581 WINNER D5. 4 v. 1.4: Final Report on Link and System Level Channel Models," Tech. Rep., 2005. [Online]. Available: <https://www.ist-winner.org>



Chi Wu received the B.E. and M.E. degrees in electronic engineering from Southeast University, Nanjing, China, in 2018 and 2021, respectively. From August 2019 to November 2019, he was a visiting student at the Department of Electrical Engineering and Electronics, University of Liverpool, U.K. His research interests include wireless localization, channel prediction, and channel modeling, with a focus on massive MIMO systems and machine learning.



Yiming Zhu received the B.E. degree in communication engineering from Nanjing University of Science and Technology, Nanjing, China, in 2020. He is currently working towards the M.E. degree with the National Mobile Communications Research Laboratory, Southeast University, Nanjing, China. His research interests include channel estimation, prediction, and modeling, with the emphasis on massive MIMO systems and statistical inference.



Cheng-Xiang Wang (Fellow, IEEE) received the B.Sc. and M.Eng. degrees in communication and information systems from Shandong University, Jinan, China, in 1997 and 2000, respectively, and the Ph.D. degree in wireless communications from Aalborg University, Aalborg, Denmark, in 2004.

He was a Research Assistant with the Hamburg University of Technology, Hamburg, Germany, from 2000 to 2001, a Visiting Researcher with Siemens AG Mobile Phones, Munich, Germany, in 2004, and a Research Fellow with the University of Agder, Grimstad, Norway, from 2001 to 2005. He has been with Heriot-Watt University, Edinburgh, U.K., since 2005, where he was promoted to a Professor in 2011. In 2018, he joined Southeast University, Nanjing, China, as a Professor. He is also a part-time Professor with Purple Mountain Laboratories, Nanjing. He has authored 4 books, 3 book chapters, and more than 450 papers in refereed journals and conference proceedings, including 25 highly cited papers. He has also delivered 23 invited keynote speeches/talks and 9 tutorials in international conferences. His current research interests include wireless channel measurements and modeling, 6G wireless communication networks, and electromagnetics information theory.

Dr. Wang is a Member of the Academia Europaea (The Academy of Europe), a Fellow of the IEEE, IET, and China Institute of Communication (CIC), an IEEE Communications Society Distinguished Lecturer in 2019 and 2020, and a Highly-Cited Researcher recognized by Clarivate Analytics in 2017-2020. He is currently an Executive Editorial Committee Member of the IEEE TRANSACTIONS ON WIRELESS COMMUNICATIONS. He has served as an Editor for nine international journals, including the IEEE TRANSACTIONS ON WIRELESS COMMUNICATIONS, from 2007 to 2009, the IEEE TRANSACTIONS ON VEHICULAR TECHNOLOGY, from 2011 to 2017, and the IEEE TRANSACTIONS ON COMMUNICATIONS, from 2015 to 2017. He was a Guest Editor of the IEEE JOURNAL ON SELECTED AREAS IN COMMUNICATIONS, Special Issue on Vehicular Communications and Networks (Lead Guest Editor), Special Issue on Spectrum and Energy Efficient Design of Wireless Communication Networks, and Special Issue on Airborne Communication Networks. He was also a Guest Editor for the IEEE TRANSACTIONS ON BIG DATA, Special Issue on Wireless Big Data, and is a Guest Editor for the IEEE TRANSACTIONS ON COGNITIVE COMMUNICATIONS AND NETWORKING, Special Issue on Intelligent Resource Management for 5G and Beyond. He has served as a TPC Member, a TPC Chair, and a General Chair for more than 80 international conferences. He received 14 Best Paper Awards from IEEE GLOBECOM 2010, IEEE ICCT 2011, ITST 2012, IEEE VTC 2013Spring, IWCMC 2015, IWCMC 2016, IEEE/CIC ICC 2016, WPMC 2016, WOCC 2019, IWCMC 2020, WCSP 2020, CSPS2021, and WCSP 2021. Also, he received the 2020 & 2021 AI 2000 Most Influential Scholar Award Honourable Mention in recognition of his outstanding and vibrant contributions in the field of Internet of Things.



Wenjin Wang (Member, IEEE) received the Ph.D. degree in communication and information systems from Southeast University, Nanjing, China, in 2011. From 2010 to 2014, he was with the School of System Engineering, University of Reading, Reading, U.K. He is currently a Professor with the National Mobile Communications Research Laboratory, Southeast University. His research interests include advanced signal processing for future wireless communications and satellite communications. He was awarded a Best Paper Award at IEEE WCSP'09. He

was also awarded the first grade Technological Invention Award of the State Education Ministry of China in 2009.



Xiqi Gao (Fellow, IEEE) received the Ph.D. degree in electrical engineering from Southeast University, Nanjing, China, in 1997.

He joined the Department of Radio Engineering, Southeast University, in April 1992. Since May 2001, he has been a professor of information systems and communications. From September 1999 to August 2000, he was a visiting scholar at Massachusetts Institute of Technology, Cambridge, and Boston University, Boston, MA. From August 2007 to July 2008, he visited the Darmstadt University of Technology, Darmstadt, Germany, as a Humboldt scholar. His current research interests include broadband multicarrier communications, massive MIMO wireless communications, satellite communications, optical wireless communications, information theory and signal processing for wireless communications. From 2007 to 2012, he served as an Editor for the IEEE TRANSACTIONS ON WIRELESS COMMUNICATIONS. From 2009 to 2013, he served as an Associate Editor for the IEEE TRANSACTIONS ON SIGNAL PROCESSING. From 2015 to 2017, he served as an Editor for the IEEE TRANSACTIONS ON COMMUNICATIONS.

Dr. Gao received the Science and Technology Awards of the State Education Ministry of China in 1998, 2006 and 2009, the National Technological Invention Award of China in 2011, the Science and Technology Award of Jiangsu Province of China in 2014, and the 2011 IEEE Communications Society Stephen O. Rice Prize Paper Award in the field of communications theory.